Smart Structures and Systems, *Vol. 30, No. 2 (2022) 209-219*
https://doi.org/10.12989/sss.2022.30.2.209

A LSTM-based method for intelligent prediction on mechanical response of precast nodular piles

Xiao-Xiao Chen [1a], Chang-Sheng Zhan [2b] and Sheng-Liang Lu*[3]

[1] *The First Affiliated Hospital of Wenzhou Medical University, Wenzhou, 325016, China*
[2] *Wenzhou Ecological Park Development and Construction Investment Group Co., Ltd, Wenzhou, 325207, China*
[3] *School of Civil Engineering and Architecture, Wenzhou Polytechnic, Wenzhou, 325000, China*

(*Received October 11, 2021, Revised May 30, 2022, Accepted July 9, 2022*)

Abstract. The determination for bearing capacity of precast nodular piles is conventionally time-consuming and high-cost by using numerous experiments and empirical methods. This study proposes an intelligent method to evaluate the bearing capacity and shaft resistance of the nodular piles with high efficiency based on long short-term memory (LSTM) approach. A series of field tests are first designed to measure the axial force, shaft resistance and displacement of the combined nodular piles under different loadings, in comparison with the single pre-stressed high-strength concrete piles. The test results confirm that the combined nodular piles could provide larger ultimate bearing capacity (more than 100%) than the single pre-stressed high-strength concrete piles. Both the LSTM-based method and empirical methods are used to calculate the shift resistance of the combined nodular piles. The results show that the LSTM-based method has a high-precision estimation on shaft resistance, not only for the ultimate load but also for the working load.

Keywords: combined nodular piles; field test; LSTM-based method; shaft resistance

1. Introduction

Soft clay soils in offshore areas are usually characterized by high compressibility and poor mechanical properties (Khanmohammadi and Fakharian 2018, Ji *et al*. 2011, Nonaka *et al*. 2017). When soft clay soil directly acts as the foundation subsoil, the infrastructure may suffer from cracking and differential settlement (Canakcila and Hamed 2017, Wu *et al*. 2020). Therefore, improvement of soft clay soil is necessary for infrastructure construction in offshore cities, such as Shanghai (Shen *et al*. 2014), Wenzhou (Wang *et al*. 2019a, Gao *et al*. 2021), and Shenzhen (Li *et al*. 2014). The ground improvement techniques mainly contain geotextiles (Sardehaei *et al*. 2019, Moradi *et al*. 2019, Zhang *et al*. 2015), prefabricated vertical drains (PVD) (Hazrati *et al*. 2020, Chai *et al*. 2018), jet grouting (Modoni and Bzówka 2012, Wang *et al*. 2018), the cast-in-site pile (Bredy and Jandora 2019, Zhou *et al*. 2016) and precast concrete piles (Altaee *et al*. 1992, Park *et al*. 2013, Horiguchi and Karkee 1995, Borda *et al*. 2007). Recently, a new type of pile combined with PHC and the nodular pile with enlarged base is developed, which is characterized with low noise, no squeezing of the soil, few mud discharge and large bearing capacity (Zhou *et al*. 2014, Wang *et al*. 2019b). The pile usually relies on the shaft resistance from soils to provide support for buildings. However, the complex interactions between the pile, mixed paste of concrete and soils, and multi-layer soils make it difficult to accurately estimate the shaft resistance.

Conventionally, the shaft resistance of the nodular pile is determined by using empirical methods or field tests. Horiguchi and Karkee (1995) proposed an empirical method for ultimate bearing capacity of nodular piles, only considering the strength of soils. Based on the method, Zhou *et al*. (2014) developed the empirical method for nodular piles with enlarged base. Most of these methods can be used only for ultimate shaft-resistance estimation by using the limit equilibrium theory. Therefore, the conventional methods only roughly estimate the ultimate shaft resistance, and are unsuitable for investigating the variation of the shaft resistance under the working load. Moreover, Various simplification rules in empirical methods, such as the simplified strata and force equilibrium, reduce the accuracy and confidence levels of estimated shaft resistance.

Alternatively, machine learning techniques are developed to determine the shaft resistance of piles. Machine learning techniques directly represent the interaction among the shaft resistance, soil, and working load without simplification. Thus, the computing results are more reliable than those of empirical methods. These machine learning techniques include neural networks (Chan *et al*. 1995, Goh 1996, Lee and Lee 1996, Teh *et al*. 1997, Abu-Kiefa 1998, Baziar *et al*. 2012, Zhang 2021a, b, c), neuro-fuzzy inference system (Ghorbani *et al*. 2018, Elbaz *et al*. 2019, Zhang *et al*. 2019), long short-term neural networks (Lu *et al*. 2020, Zhang *et al*. 2021a, b, c, d, Tang

*Corresponding author, Ph.D., Professor,
E-mail: 2009230009@wzpt.edu.cn
[a] Senior Engineer, E-mail: 150506564@qq.com
[b] Senior Engineer, E-mail: 645363087@qq.com

Copyright © 2022 Techno-Press, Ltd.

ISSN: 1738-1584 (Print), 1738-1991 (Online)

et al. 2021), and other machine learning methods (Zhang *et al*. 2020a, b, Ye *et al*. 2020, Ni *et al*. 2017, Zhang 2008). The LSTM method is able to consider the interaction among different strata using specified gate cells (Gao *et al*. 2020). Recently, the LSTM network is also employed in civil engineering for other problems, e.g., soil moisture estimation (Fang *et al*. 2019), determination of the hydromechanical coupling effect of porous media (Wang and Sun 2018), concrete strength evaluation (Dutta *et al*. 2018, Ozcan *et al*. 2017) and stress-strain behaviour. However, the above studies only used the typical mean square error (MSE) cost function, which ignored the numerical difference between multi-scale samples and would arise unfair bias in low-value samples (Zhang *et al*. 2019).

This study aims to evaluate the shaft resistance of precast nodular piles with enlarged piles in soft clay soils via field tests, using the LSTM method with REMSE cost function. First, field tests were designed and conducted to investigate the shaft resistance and axial force of precast nodular piles under different loads in soft clay, in Shanghai, China. Then, the empirical methods were used to estimate the ultimate bearing capacity of the pile, and the results were compared with the measured data. Subsequently, an LSTM method was developed and employed to predict the shaft resistance and axial force of the pile, not only under the working load but also under the ultimate load.

2. Field experiment and measurement

The field experiments were conducted in the clay ground of the Caihong hospital, in Shanghai, China. The soft clays in the field were laid layer by layer, which were <1> backfill, <2> sandy clay, <3> mud clay, <4> extra-soft silty clay, <5-1> soft silty clay, <5-2> silty clay with silt, <5-3> medium silty clay, <6> dense silty clay, <7> silty clay, <8> silty clay with sand, <9> dense silty sand, respectively, from top to bottom. Fig. 1 shows the simplified geological profile in the field. Soft soils in the field were mainly silty clays and sands. The soil properties are further evaluated using laboratory tests e.g., triaxial undrained consolidation test and routine analysis tests. Fig. 2 presents the basic mechanical and physical properties of soils.

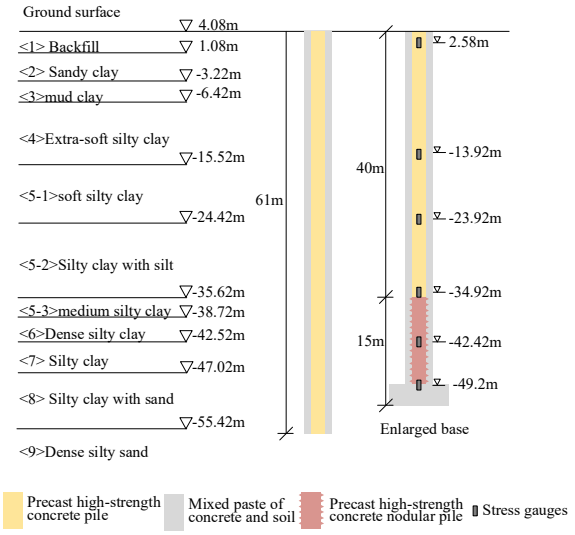

Fig. 1 Geological profile in the filed

2.1 Experiment scenario

In total, three new combined piles, which were comprised of precast high-strength concrete (PHC) pile and precast concrete enlarged-base nodular (PCN), were built for the evaluation of bearing capacity. Besides, three single PHC piles were also constructed for comparison. The total lengths of new combined piles were 55m, which contained 40 m of PHC pile and 15 m of PCN pile, as shown in Fig. 1. The average length of single PHC piles was 61 m. The diameters of PHC piles were 600 mm. The diameters of nodular joints of PCN piles were 650 mm, and the diameters of non-nodular joints of PCN piles were 500 mm. The enlarged bases of combined piles were 1200 mm in diameter and 2750 mm in height. Fig. 3(a) shows the layout of three combined piles of PHC and PCN piles (named as P1-1, P1-2, P1-3), and three single PHC piles (named as P2-1, P2-2, P2-3). The compressive strengths of high-strength concrete of piles were 80 Mpa. The weight ratio of concrete and water in the mixed pasted around the precast piles was 1. The measured unconfined compressive strengths of the mixed paste of concrete and water ranged from 1. 72 to 4. 01 MPa, based on the laboratory tests. The compressive modulus of the enlarged base was estimated as 2500 MPa by experience (Wang *et al*. 2019a, b).

After 43 or 45 days of all piles are constructed, static load tests were implied step by step to investigate the ultimate loading capacity of piles. Figs. 3(b) and (c) briefly shows the static load test system. The initial load was 1600 kN, and then increased 800 kN at each step until the pile collapsed. The test will stop when the displacement of the pile at the next load is twice the displacement at the former load and the pile behaves continuous deformation for 24 hours according to the Chinese code JGJ106-2014 (MOHURD 2014). The loads were then unloaded by 1600

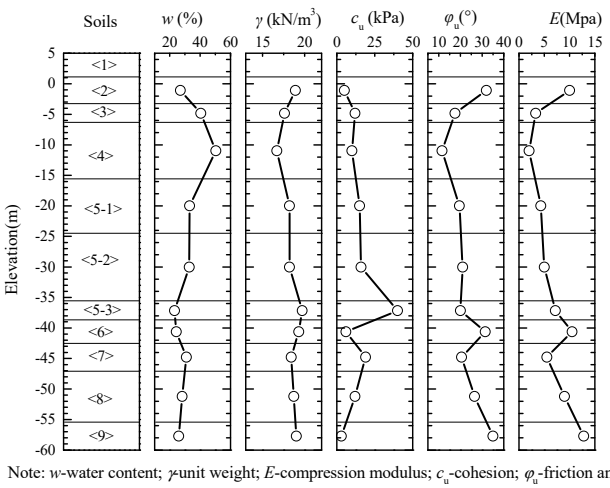

Note: w-water content; γ-unit weight; E-compression modulus; c_u-cohesion; φ_u-friction angle

Fig. 2 Mechanical and physical properties of soils in the field

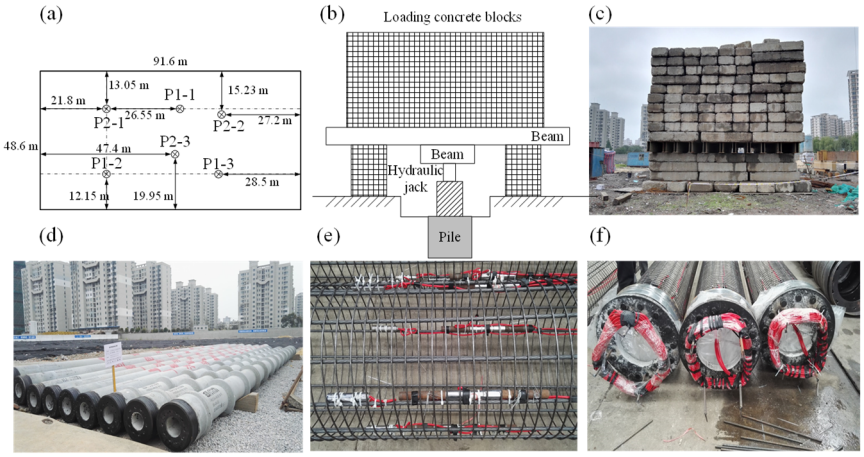

Fig. 3 Sketch of the field test program and site photos: (a) layout of piles; (b) design of static loading system; (c) static loading system on site; (d) nodular pile; (e) bound stress gauges; (f) wires of stress gauges

kN at each step. At each load step, the settlements of piles were measured at 5 min, 15 min, 30 min, 45 min, 60 min, and then at a fixed interval of 30 min, until the piles stabilized. At each unloading step, the displacements of piles were recorded at 5 min, 15 min, 30 min, 60min, respectively.

The combined piles were instrumented with six stress gauges to measure the axial force of the pile, at depths of 1.5 m, 18 m, 28 m, 39 m, 46.5 m, 53.5 m, respectively. The stress gauges were bound to the steel reinforcement cage as shown in Figs. 3(e) and (f). Since the backfill in the field was loose and low-strength, the shaft resistance from the backfill was then ignored.

2.2 Experimental results

2.2.1 Load-displacement response

Fig. 4 shows the curves of loads and settlements of combined piles and single PHC piles in the static load tests. This suggests that the soils around the piles underwent plastic deformation and the pile tip resistances increased. For the combined piles, the settlements of piles gradually increase with the static loads without rapid variation, which are defined as the gradual-variation type in the Chinese code JGJ106-2014 (MOHURD 2014). The ultimate load is estimated as 8800 where the total settlement surpasses 40 mm, according to the same Chinese code. For single PHC piles, the settlements have rapid increases when the loads are over 3000 kN. Therefore, the ultimate load of PHC piles is estimated as 3000 kN. The ultimate loads of new combined piles are twice more than those of PHC piles. Generally, the combined piles could provide enough support to the upper infrastructures according to the load-displacement response.

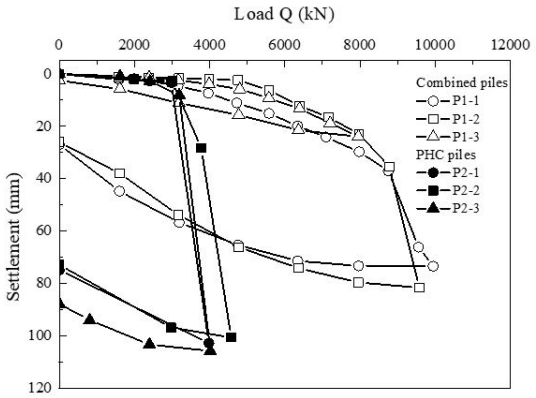

Fig. 4 Curves of load and settlement of piles in static load tests

2.2.2 Axial force

The axial forces of combined piles were monitored by using the pre-instrumented stress gauges as shown in Fig. 1. Fig. 5 depicts the measured axial forces of three combined piles under different loads. Under each load, the axial forces of the three piles generally decreased with the depth, which means the shaft resistance of different soils works together to support the load. It could be observed that the slopes of axial forces at the top of the pile were almost the same after 3200 kN, where soils had low strengths as shown in Fig. 2. This phenomenon illustrates that the shaft resistance from the soft soils had already arrived the ultimate capability at the load of around 3200 kN. As the increase of loads, the shaft resistance of this part of the pile had no change any more. On the contrary, the slopes of axial force kept decreasing when depths were larger than 20 meters under different loads. The decreasing slope of axial forces implied the increase of shaft resistance of pile. In addition, the axial forces at the end of the pile increased with the loads, which indicated that the tip resistance of the pile gradually developed. The tip resistance provided nearly 2000 kN, which was around 20-25 percent of the total ultimate load (estimated as 8800 kN).

It was observed that there were apparent turning points at the intersection between the PHC piles and PCN piles to most of axial force curves under different loads. For the PHC part of the combined piles, the slopes of axial force curves gradually stabilized after the loads over 6000 kN, as shown in Fig. 5. The stabilized slopes implied that the shaft resistances of PHC piles had provided the ultimate bearing capacity, and thus would not increase any more. Regarding

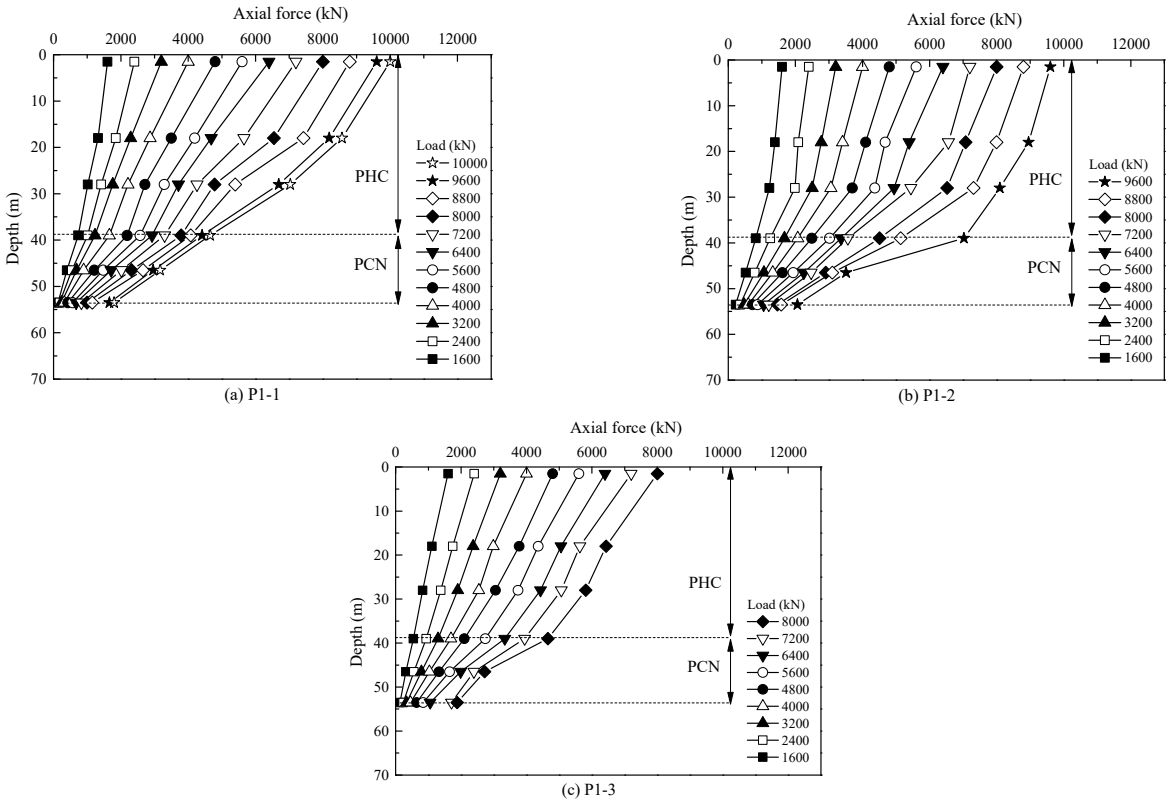

Fig. 5 Axial force development under different loads of combined piles

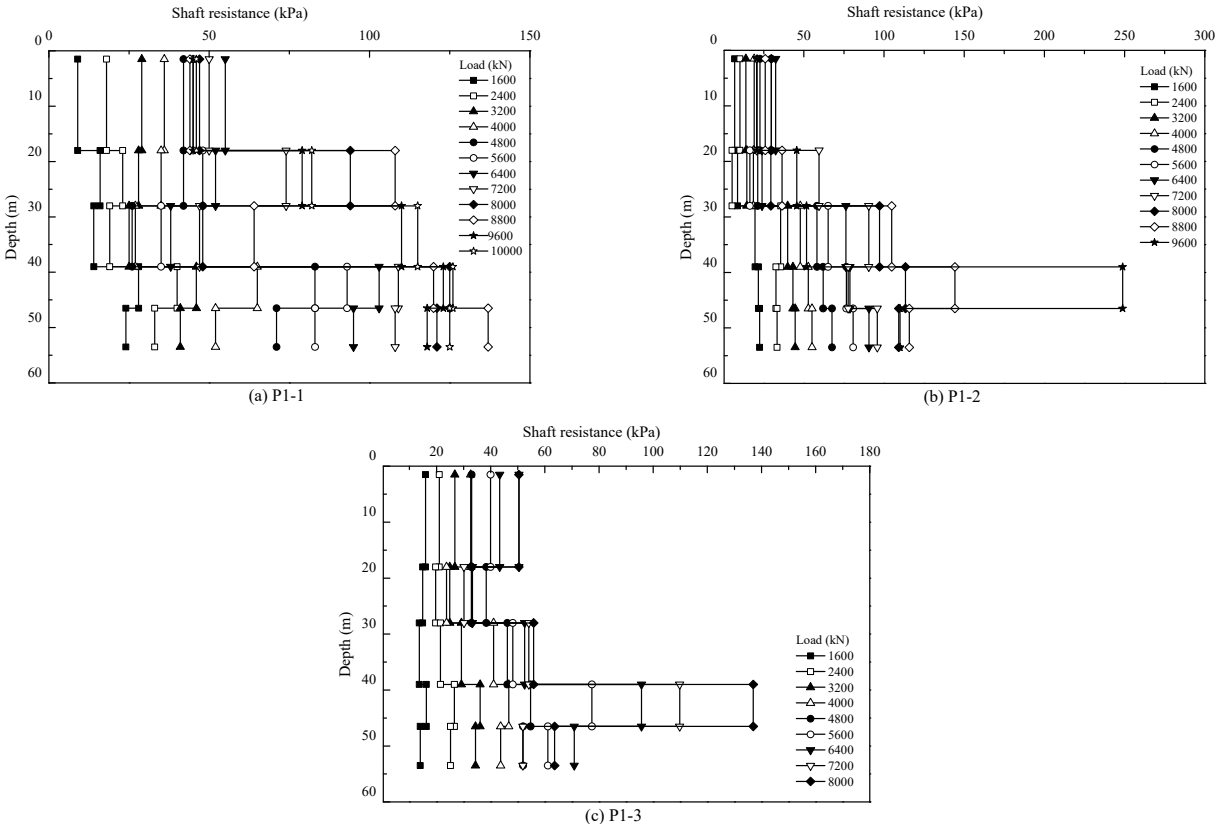

Fig. 6 Shaft resistance under different loads of three combine piles

the PCN piles of the combined piles, the slopes of axial forces kept increasing with the loads. This is attributed to the increasing shaft resistances of the PCN piles.

2.2.3 Shaft resistance

The shaft resistance τ_i of the combined pile at the i^{th} layer of soils was computed by using Eq. (1).

$$\tau_i = (N_i - N_{i-1})/(h_i p) \tag{1}$$

where, N_i is the axial force at the top of the i^{th} layer of soil, h_i is the thickness of the i^{th} layer of soil and p is the circle of the pile.

Fig. 6 depicts the shaft resistance of three combined piles under different loads. The shaft resistances of piles at the top of 20 meters have few variations after the load was over 6400 kN. Which was consistent with the results of the axial forces in Fig. 5. Generally, the shaft resistance of pile increased with the depth under different load. The shaft resistances of PCN piles were larger than those of PHC piles, especially for P1-2 and P1-3 whose peak shaft resistance of PCN piles could arrive at 250 kPa. It could be seen that pile P1-1 and P 1-2 arrived at the ultimate shaft resistance at most of soil layers under the load of 8800 kN. The shaft resistance reduced when the load continued increasing, which was probably due to the plastic yield of soils. Even though the pile P1-3 still worked under the load of 8000 kN without reaching the ultimate shaft resistance, it was reasonably inferred that the combined piles would arrive at the ultimate shaft resistance under the load of 8800 kN, which was consistent with the load-displacement response in Fig. 4.

3. Empirical method

Considering the similarity of P1-2, P1-2 an P1-3, only P1-1 is evaluated the ultimate shaft resistance by using the empirical method. The empirical methods include the α method (Randolph and Murphy 1985) and the β method (Ling *et al*. 2018) as follows.

$$\begin{matrix} \tau u & \text{method}_{max} \\ \tau'_{v_0}{}' \tan\varphi & \text{method}_{max} \end{matrix} \tag{2}$$

where, τ_{max} is the ultimate shear resistance of the pile; S_u is the undrained shear strength of soils; σ'_v is the vertical effective stress; φ is the friction angle; α value is determined by the API method (Randolph and Murphy 1985) as (3).

$$\alpha = 0.5\left(\frac{S_u}{\sigma_v'}\right)^{-0.5} \tag{3}$$

K_0 is the coefficient of earth pressure at rest as below (Mayne and Kulhawy 1982).

$$K_0 = (1 - \sin\varphi)OCR^{\sin\varphi} \tag{4}$$

where OCR is the over-consolidation ratio, for normally consolidated soils in this case, OCRs of soils are always equal to 1; The undrained shear strength of the soil S_u is computed as follows (Ma *et al*. 2014).

$$S_u = c + \sigma_3 \tan\varphi \tag{5}$$

where, c_u is the cohesion under undrained conditions; σ_3 is the minimum main stress of the soil, which is estimated as below

$$\sigma_3 = \frac{1 + 2K_0}{3}\sigma_v' \tag{6}$$

The estimated undrained shear strengths of soils are shown in Fig. 7, which generally increases with the depth.

The estimated shaft resistances of the pile P1-1 are separately calculated by the α method and the β method, as shown in Fig. 8. In general, the results of the empirical methods are in rough accordance with the measured shaft resistances. However, biases arise for both empirical methods when the depth is less than 30 meters. The root square mean errors (RMSEs) are 33.48 kPa and 32.95 kPa for the α method and the β method, respectively. The RMSEs are nearly 30 percent of the maximum measured shaft resistance of 100 kPa. In addition, the α method approaches more to the measured results than the β method at the depth more than 30 meters. Those biases imply that the empirical methods with the ideal hypothesis are not suited to represent the ultimate shaft resistance of the combined piles.

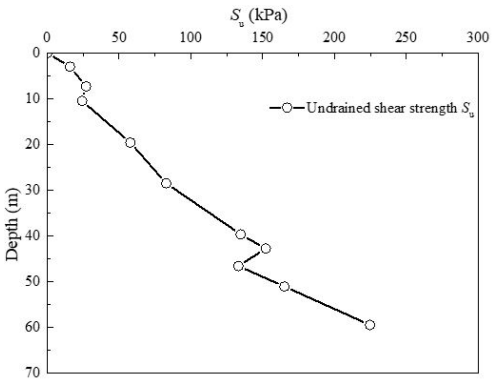

Fig. 7 Undrained shear strength S_u of soils in the filed site

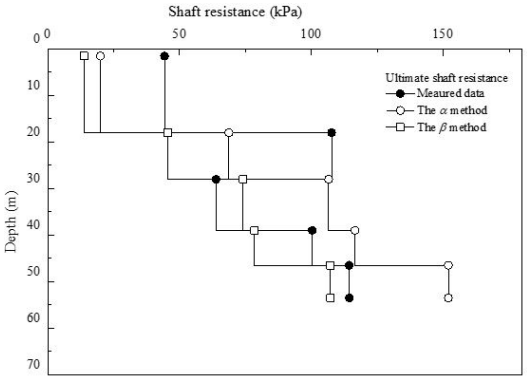

Fig. 8 Shaft resistance under different loads of the combined pile P1-1

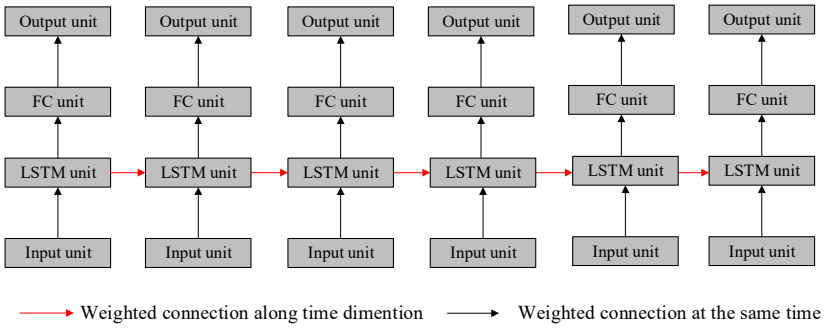

Fig. 9 Two-layered topology structures of the LSTM method

4. LSTM-based approach

4.1 Methodology

The long short-term memory (LSTM) machine learning technique is adopted to evaluate the nonlinear axial forces of the combined piles. The shaft resistance would be then computed by using the estimated axial forces. Different from the empirical methods, the LSTM machine learning technique represent the axial force of piles from data of the field test. Fig. 9 shows the two-layered topology structures of LSTM networks. The LSTM networks are comprised of input units, LSTM units, fully connected (FC) units, and output units, respectively. The key for learning sequenced behaviors is a special unit called the LSTM unit. The LSTM units interconnect each other along time dimension to reflect the interaction of the historical data on the current or future data.

The typical LSTM unit is usually composed of input gate, output gate, forget gate and unit input Supposed $\boldsymbol{X}^t$ as the input data and $\boldsymbol{y}_L{}^t$ as the output data of simplified LSTM unit at time t. After the input data $\boldsymbol{X}^t$ and historical data $\boldsymbol{y}^{t-1}$ are imported into LSTM units, the calculation process is formulated as below.

$$\begin{aligned}
&\overline{\boldsymbol{i}^t} = \boldsymbol{W}_i \times \boldsymbol{X}^t + \boldsymbol{R}_i \times \boldsymbol{y}_L{}^{t-1} + \boldsymbol{b}_i \quad \Rightarrow \quad \mathbf{i}^t = S(\overline{\boldsymbol{i}^t}) \\
&\overline{\boldsymbol{f}^t} = \boldsymbol{W}_f \times \boldsymbol{X}^t + \boldsymbol{R}_f \times \boldsymbol{y}_L{}^{t-1} + \boldsymbol{b}_f \quad \Rightarrow \quad \mathbf{f}^t = S(\overline{\boldsymbol{f}^t}) \\
&\overline{\boldsymbol{o}^t} = \boldsymbol{W}_o \times \boldsymbol{X}^t + \boldsymbol{R}_o \times \boldsymbol{y}_L{}^{t-1} + \boldsymbol{b}_o \quad \Rightarrow \quad \mathbf{o}^t = S(\overline{\boldsymbol{o}^t}) \\
&\overline{\boldsymbol{z}^t} = \boldsymbol{W}_z \times \boldsymbol{X}^t + \boldsymbol{R}_z \times \boldsymbol{y}_L{}^{t-1} + \boldsymbol{b}_z \quad \Rightarrow \quad \mathbf{z}^t = T(\overline{\boldsymbol{z}^t}) \\
&\boldsymbol{c}^t = \boldsymbol{i}^t \odot \boldsymbol{z}^t + \boldsymbol{c}^{t-1} \odot \boldsymbol{f}^t \\
&\boldsymbol{y}_L{}^t = T(\boldsymbol{c}^t) \odot \boldsymbol{o}^t
\end{aligned} \tag{7}$$

where $\boldsymbol{W}_i$, $\boldsymbol{W}_o$, $\boldsymbol{W}_f$ and $\boldsymbol{W}_z$ are weights of input data of input gate, output gate, forget gate and input unit, respectively. $\boldsymbol{R}_i$, $\boldsymbol{R}_o$, $\boldsymbol{R}_f$ and $\boldsymbol{R}_z$ are recurrent weights of recurrent data of input gate, output gate, forget gate and input unit, respectively. $\boldsymbol{b}_i$, $\boldsymbol{b}_o$, $\boldsymbol{b}_f$ and $\boldsymbol{b}_z$ are bias weights of input gate, output gate, forget gate and input unit, respectively. $\boldsymbol{i}^t$ and $\boldsymbol{i}^t$ refer to the input and output data of the input gate. $\boldsymbol{f}^t$ and $\boldsymbol{f}^t$ refer to the input and output data of the forget gate. $\boldsymbol{o}^t$ and $\boldsymbol{o}^t$ refer to the input and output data of the output gate. $\boldsymbol{z}^t$ and $\boldsymbol{z}^t$ refer to the input and output data of the input unit. $\boldsymbol{c}^t$ means the cell stage of the LSTM unit while $\boldsymbol{y}_L{}^t$ means the output data of the LSTM unit. S is the sigmoid activation function. T is hyperbolic tangent activation function.

Table 1 Example of the input data of the LSTM model

The input data					
Depth (m)	K_0	σ'_v (kPa)	c_u (kPa)	φ_u (°)	S_u (kPa)
1.5	0.47	13.35	5	32	15.79
18	0.67	155.44	15	19.5	57.79
28	0.64	228.42	16	21	82.73
39	0.66	337.06	40	20	134.71
46.5	0.65	397.81	19	20.5	133.01
53.5	0.55	436.96	12	26.5	165.05

4.2 Modelling details

The modelling procedure of the LSTM approach mainly contains data preparation, architecture determination and optimization process.

Regarding the preparation of data, the input data should include the earth pressure coefficient K_0, the vertical effective stress σ'_v, the cohesion c_u, the friction angle φ_u, the undrained shear strength S_u, the thickness of each layer of soil and the load. Table 1 tabulates the input data for all layers of soils. The input data are generally constituted of soil properties, physical properties and the load, which are highly correlated to the shaft resistance of piles. The output data include the axial force and the shaft resistance of the combined pile under different loads. The input and output data would be normalized to the range from 0 to 1 through dividing the maximum values, before imported into the LSTM networks. Therefore, the dataset is consisted of 12 sets of measured data under the loads of 1600 kN, 2400 kN, 3200 kN, 4000 kN, 4800 kN, 5600 kN, 6400 kN, 7200 kN, 8000 kN, 8800 kN, 9600 kN, 10000 kN, respectively. 8 sets of data are specified as the training set, which are 1600 kN, 2400 kN, 3200 kN, 4000 kN, 4800 kN, 6400 kN, 8000 kN, 9600 kN, respectively, while the others are the testing set.

The LSTM network is consisted of two hidden layers with the twelve hidden nodes at each layer. The number of nodes in the hidden layers are determined using the trial-and-error method. The cost function J is designated as the relative mean square error (REMSE) function as follows.

$$J_{REMSE} = \frac{1}{2N} \times \sum_{i}^{N} \left(\frac{y_{pi} - y_i}{y_i} \right)^2 + \frac{\lambda}{2N} \tag{8}$$

$$\times\left(\sum W^{1}+\sum W^{2}\right) \tag{8}$$

where N is the number of training samples. λ is the regularization parameter which provides punishment to weights W^1 and W^2 to prevent overfitting (defined as 0.1 in this case). The REMSE cost function is first proposed by Zhang (2019), which is prior to multi-scale assignments.

The conjugate gradient descent algorithm is adopted as the optimization algorithm to train the LSTM network. Wolfe-Powell criterion and linear search method are applied for precise gradient descent. The total amount of iterations is specified as 3000 which is enough for this case by experience (Lu *et al*. 2020).

4.3 data augment

The original dataset from the field experiments only contains 12 data sets. The size of dataset is so few for a deep learning method, which tend to arise an overfitting problem and reduce the reliability of deep learning model.

In this study, we introduced a gaussian error of 1% to the original dataset and then synthetise an enlarged dataset with 160 sets of training data. The enlarged dataset would help to relieve the overfitting problem from a small dataset. Fig. 10 present the error distribution of the axial force and shaft resistance in the enlarged dataset. The LSTM model trained by using the enlarged dataset would refer as En-LSTM model.

In the future, more data of piles would be collected from other projects to update the measured dataset. The proposed model would be captured more accurate relationship among the load, ground and piles. Therefore, the reliability and accuracy of proposed deep learning model would increase with the update of dataset.

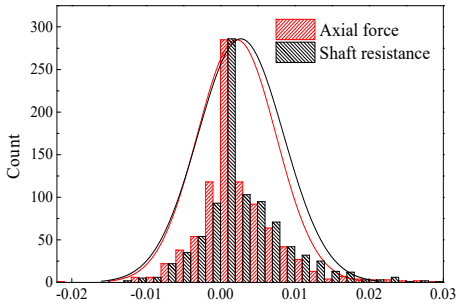

Fig. 10 Error distribution of enlarged dataset

4.4 Result and analysis

The results of the LSTM method are assessed by the root square mean error (RMSE) and coefficient of determination (R^2). Larger coefficient of determination and less root square mean error means better prediction performance. The definition of RMSE and R^2 are given in Eq. (9), respectively.

$$RMSE=\sqrt{\frac{1}{N}\sum_{i}^{N}(y_{pi}-y_i)^2}$$
$$R^2=1-\frac{\sum_i^N(y_i-y_{pi})^2}{\sum_i^N(y_i-\bar{y})^2} \tag{9}$$

where i is the i^{th} set of input data, N is the number of training or testing samples, y_i is the i^{th} set of measured ground settlements, y_{pi} is the i^{th} set of predicted ground settlements, and $\bar{y}$ is the mean value of measured ground settlements.

Figs. 11 and 12 present the training and testing results of the axial force and shaft resistance of the LSTM method, respectively. Generally, the LSTM method has an excellent capability in determining axial forces and shaft resistances of the combined piles. The training results of the LSTM method are tightly associated with the measured data. After trained by measured data, the LSTM method accurately predicted the axial forces and shaft resistances under unexpected loads. In comparison with the results of the empirical methods in Fig. 8, the ultimate shaft resistances under 8800 kN predicted by the LSTM method are much more precise. Therefore, the LSTM method is an applicable approach to determine the axial force and shaft resistance of the cast-in-site piles, which outperforms the empirical method by high precision.

By introducing gaussian error to augment the original dataset, the predictive capability of LSTM model is further improved as shown in Fig. 12. Table 2 shows the R^2s and

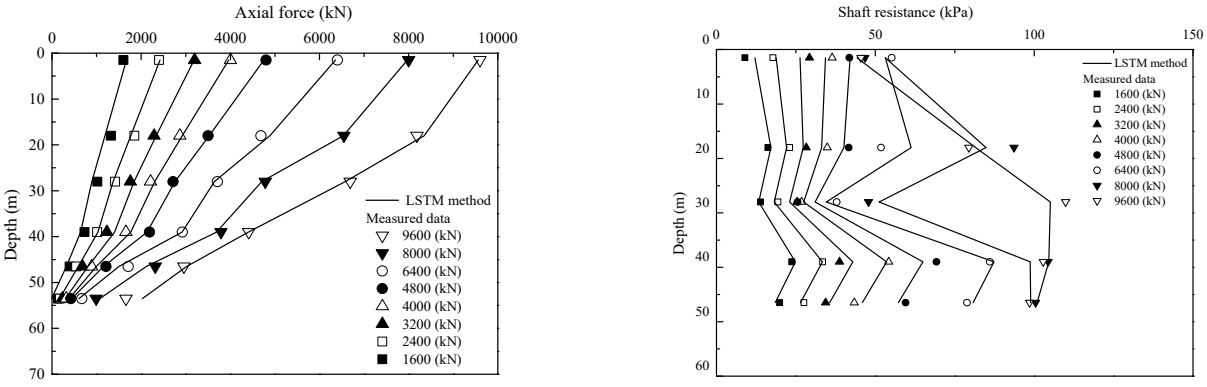

(a) Axial force (b) Shaft resistance

Fig. 11 Training performance of the LSTM method under different loads of pile P1-1 on original dataset

problem resulting from a small dataset.

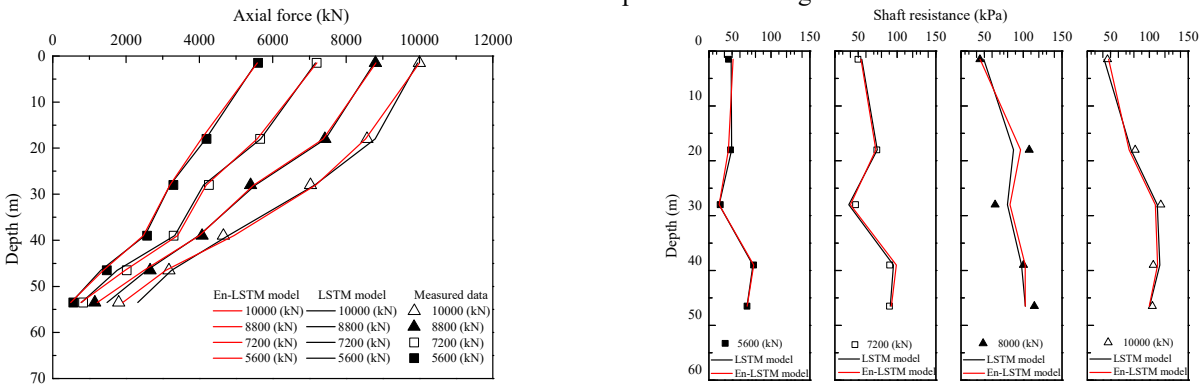

(a) Axial force (b) Shaft resistance

Fig. 12 Prediction of the LSTM method under different loads of pile P1-1 on original dataset and enlarged dataset

Table 2 Evaluation indices of the performances of the LSTM model

Dataset	Load (kN)	LSTM model				En-LSTM model			
		R^2		RMSE		R^2		RMSE	
		A*	S	A (kN)	S (kPa)	A	S	A (kN)	S (kPa)
Training	1600	0.962	0.956	109	1.68	0.997	0.987	30.9	0.74
	2400	0.989	0.966	44.4	0.95	0.999	0.968	29.7	0.42
	3200	0.999	0.977	99.2	2.64	0.997	0.981	29.9	2.54
	4000	0.995	0.979	81.3	1.72	1.000	0.994	15.0	1.13
	4800	0.998	0.978	43.5	3.34	0.999	0.999	77.2	3.11
	6400	0.996	0.996	125	4.68	0.999	0.999	41.4	2.53
	8000	0.996	0.993	103	5.72	0.998	0.999	61.1	0.82
	9600	0.995	0.99	172	2.76	1.000	0.995	74.0	1.20
Testing	5600	0.997	0.995	85.8	1.8	0.997	0.988	94.8	3.0
	7200	0.997	0.981	126	5	0.999	0.980	70.4	5.2
	8800	0.996	0.895	156	12.8	0.999	0.926	88.5	11.3
	10000	0.992	0.985	244	5.4	0.998	0.982	144.1	5.7

*A: axial force; S: shaft resistance

RMSEs of the training and testing results of the LSTM model and En-LSTM model. For the LSTM model, most of R^2s of the axial force are more than 0.99 for both the training and testing dataset. The R^2s of the shaft resistance are also more than 0.89 under different loads. In addition, the maximum RMSE of the predictive axial forces is only 170 kN, which is less than 3 percent of the ultimate loads 8800 kN. The maximum error of the shaft resistance is less than 6 kPa for training dataset and less than 13 kPa for testing dataset. The RMSE of the predictive ultimate shaft resistance of the combined pile is only 12.8 kPa, which is far less than those of empirical methods. In conclusion, the high R^2s and small RMSEs illustrate that the LSTM method is capable of learning and predicting the axial force and shaft resistance of the combined piles with enlarged piles. For the En-LSTM model, the R^2 are generally higher and RMSEs are lower than the LSTM model for both training and testing datasets. Therefore, the enlarged dataset with gaussian errors is valid in alleviating the overfitting

5. Discussion

In general, empirical methods can roughly estimate the scale of the ultimate mechanical response of piles, as illustrated in Fig. 8. By multiplying a scaling safety factor of ≥ 1.5 with the estimated ultimate shaft resistance, the empirical results can guide the bearing capacity design of piles in soft ground, and this approach is currently common when constructing piles. However, the piles tend to provide excessive bearing capacity, which not only increases the cost but also delays the schedule. In contrast, our proposed method can estimate the mechanical response of piles with much higher precision than empirical methods based only on limited field data, as illustrated in Fig 12. Precise prediction aids the effective and safe design of the ultimate shaft resistance of piles. In addition, for increased accuracy of testing of the intelligent method under different working loads, the number of steps of the static load test can be reduced from 12 to 8 load steps. The reduction of load steps

would can also reduce the time required for the processing stage considerably. Therefore, the proposed intelligent method is a promising tool to guide the effective design of piles in soft ground in offshore areas.

6. Conclusions

Based on the field tests, this study proposes an intelligent method to evaluate the axial force and shaft resistance of the combined piles of the PHC piles and PCN piles. Conclusions are summarized as follows:

- The empirical method suffered large errors from computing the ultimate shaft resistances of the combined piles. The RMSEs were 33.48 kPa and 32.95 kPa for the α method and the β method, respectively, which were nearly 30 percent of the maximum measured shaft resistance of 100 kPa.
- A novel intelligent method is proposed based on the LSTM method with REMSE cost function to accurately estimate the axial force and shaft resistance, not only under the ultimate bearing state but also under the normal working state of the pile. The RMSE of the predictive ultimate shaft resistance of the combined pile is only 12.8 kPa, around 10 percent of the measured data. The R^2s of the shaft resistance are also more than 0.89 under different loads.
- A data augment method by introducing gaussian error is evidenced as valid for alleviating the over fitting issue resulting from a small dataset. The En-LSTM with enlarged dataset is prior to the LSTM with original small dataset in both R2 and RMSE on training and testing datasets.

Acknowledgments

The research described in this paper was financially supported by the research fund of Wenzhou Polytechnic (No. WZY2020003) and Wenzhou Ecological Park Management Committee (No. sty2020002). The source of financial support is gratefully acknowledged.

References

Abu-Kiefa, M.A. (1998), "General regression neural networks for driven piles in cohesionless soils", *J. Geotech. Geoenviron. Eng.*, *ASCE*, **124**(12), 1177-1185. https://doi.org/10.1061/(ASCE)1090-0241(1998)124:12(1177)

Altaee, A., Fellenius, B.H. and Evgin, E. (1992), "Axial load transfer for piles in sand I: tests on an instrumented precast pile", *Can. Geotech. J.*, **29**(1), 11-20. https://doi.org/10.1139/t92-002

Baziar, M.H., Kashkooli, A. and Saeedi-Azizkandi, A. (2012), "Prediction of pile shaft resistance using cone penetration tests (CPTs)", *Comput. Geotech.*, **45**, 74-82. https://doi.org/10.1016/j.compgeo.2012.04.005

Borda, O., Uno, M. and Towhata, I. (2007), "Shaft capacity of nodular piles in loose sand", *Proceedings of the 49th National Conference*, *Japanese Geotechnical Society*, Vol. 2, pp. 175-176. [In Japanese]

Bredy, S. and Jandora, J. (2019), "Three-Dimensions Modelling of a Jet Pile Construction in the Karolinka Dam", *Acta Universitatis Agriculturae et Silviculturae Mendelianae Brunensis*, **67**(3), 637-648. https://doi.org/10.11118/actaun201967030637

Canakcila, H. and Hamed, M. (2017), "Experimental study on axial response of different pile materials in organic soil", *Geomech. Eng., Int. J.*, **12**(6), 899-917. http://doi.org/10.12989/gae.2017.12.6.899

Chai, J.C., Shen, J.S.L., Liu, M.D. and Yuan, D.J. (2018), "Predicting the performance of embankments on PVD-improved subsoils", *Comput. Geotech.*, **93**, 222-231. https://doi.org/10.1016/j.compgeo.2017.05.018

Chan, W.T., Chow, Y.K. and Liu, L.F. (1995), "Neural network: an alternative to pile driving formulas", *Comput. Geotech.*, **17**(2), 135-156. https://doi.org/10.1016/0266-352X(95)93866-H

Dutta, S., Samui, P. and Kim, D. (2018), "Comparison of machine learning techniques to predict compressive strength of concrete", *Comput. Concrete, Int. J.*, **21**(4), 463-470. https://doi.org/10.12989/cac.2018.21.4.463

Elbaz, K., Shen, S.L., Zhou, A.N., Yuan, D.J. and Xu, Y.S. (2019), "Optimization of EPB shield performance with adaptive neuro-fuzzy inference system and genetic algorithm", *Appl. Sci.*, **9**(4), 780. https://doi.org/10.3390/app9040780

Fang, K., Pan, M. and Shen, C.P. (2019), "The value of SMAP for long-term soil moisture estimation with the help of deep learning", *IEEE Transact. Geosci. Remote Sens.*, **57**(4), 2221-2233. https://doi: 10.1109/TGRS.2018.2872131

Gao, M.Y., Zhang, N., Shen, S.L. and Zhou, A. (2020), "Real-time dynamic earth-pressure regulation model for shield tunneling by integrating GRU deep learning method with GA optimization", *IEEE Access*, **8**, 64310-64323. https://doi.org/10.1109/ACCESS.2020.2984515

Gao, Y., Li, Z., Sun, D.A. and Yu, H.H. (2021), "A simple method for predicting the hydraulic properties of unsaturated soils with different void ratios", *Soil Tillage Res.*, **209**, 104913. https://doi.org/10.1016/j.still.2020.104913

Ghorbani, B., Sadrossadat, E., Bazaz, J.B. and Oskooei, P.R. (2018), "Numerical ANFIS-based formulation for prediction of the ultimate axial load bearing capacity of piles through CPT data", *Geotech. Geol. Eng.*, **3**, 1-20. https://doi:10.1007/s10706-018-0445-7

Goh, A.T.C. (1996), "Pile driving records reanalyzed using neural networks", *J. Geotech. Geoenviron. Eng.*, *ASCE*, **122**(6), 492-495. https://doi.org/10.1061/(ASCE)0733-9410(1996)122:6(492)

Hazrati, H., Karimi, N. and Jafarzadeh, Y. (2020), "Performance and antifouling properties of PVDF/PVP and PSf membranes in MBR: A comparative study", *Membr. Water Treat., Int. J.*, **11**(2), 159-166. http://doi.org/10.12989/mwt.2020.11.2.159

Horiguchi, T. and Karkee, M.B. (1995), "Load tests on bored PHC nodular piles in different ground conditions and the bearing capacity based on simple soil parameters", *Proceedings of Technical Report of Japanese Architectural Society*, pp. 89-94. https://doi.org/10.3130/aijt.1.89

Ji, F., Ding, J.W., Hon,g Z.S. and Gui, Y. (2011), "Experimental study on dewatering dredged clay with ventilating vacuum method", *Adv. Mater. Res.*, **5**, 261-263. https://doi.org/ 10.4028/www.scientific.net/AMR.261-263.1650

Khanmohammadi, M. and Fakharian, K. (2018), "Evaluation of performance of piled-raft foundations on soft clay: A case study", *Geomech. Eng., Int. J.*, **14**(1), 43-50. https://doi.org/10.12989/gae.2018.14.1.043

Lee, I.M. and Lee, J.H. (1996), "Prediction of pile bearing capacity using artificial neural networks", *J. Comput. Geotech.*, **18**(3), 189-200. https://doi.org/10.1016/0266-352X(95)00027-8

Li, A.G., Tham, L.G., Wen, J.P. and Chen, S.C. (2014), "Case

study of ground improvement to Qianhai reclamation area", In: *Ground Improvement and Geosynthetics*, Geotechnical Special Publication, Qianhai Bay, Shenzhen, China, pp. 231-240. https://doi.org/10.1061/9780784413401.023

Ling, Z., Wang, W., Wu, J., Huang, M. and Yuan, J. (2018), "Shaft resistance of pre-bored precast pile in shanghai clay", *Proceedings of the ICE - Geotechnical Engineering*, pp. 1-47. https://doi.org/10.1680/jgeen.18.00028

Liu, H.B., Zhang, Q. and Zhang, B.H. (2017), "Structural health monitoring of a newly built high-piled wharf in a harbor with fiber Bragg grating sensor technology: Design and deployment", *Smart Struct. Syst., Int. J.*, **20**(2), 163-173. https://doi.org/10.12989/sss.2017.20.2.163

Lu, S.L., Zhang, N., Shen, S.L., Zhou, A. and Li, H.Z. (2020), "A deep-learning method for evaluating shaft resistance of the cast-in-site pile on reclaimed ground using field data", *J. Zhejiang Univ.-SCIENCE A*, **21**(6), 496-508. https://doi.org/10.1631/jzus.A1900544

Ma, H.P., Chen, Z.Y. and Yu, S. (2014), "Correlations of soil shear strength with specific penetration resistance of CPT in shanghai area", *Yantu Lixue/Rock and Soil Mechanics*, **35**(2), 536-542. https://doi.org/10.16285/j.rsm.2014.02.021

Mayne, P.W. and Kulhawy, F.H. (1982), "K0-OCR relationships in soil", *J. Geotech. Eng. Div.*, **108**(6), 851-872. https://doi.org/10.1061/AJGEB6.0001306

Modoni, G. and Bzówka, J. (2012), "Analysis of foundations reinforced with jet grouting", *J. Geotech. Geoenviron. Eng.*, **138**(12), 1442-1454. https://doi.org/10.1061/(ASCE)GT.1943-5606.0000718

Moradi, G., Abdolmaleki, A. and Soltani, P. (2019), "Small-and large-scale analysis of bearing capacity and load-settlement behavior of rock-soil slopes reinforced with geogrid-box method", *Geomech. Eng., Int. J.*, **18**(3), 315-328. https://doi.org/10.12989/gae.2019.18.3.315

MOHURD (Ministry of Housing and Urban-Rural Devel-opment of the People's Republic of China) (2014), Technical Code for Testing of Building Foundation Piles, JGJ106-2014, National Standards of the People's Republic of China. [In Chinese]

Nonaka, T., Yamada, S. and Noda, T. (2017), "Soil-water coupled analysis of pore water pressure dissipation in performance design-examinations of effectiveness in reclaimed ground", *Geotech. Eng.*, **48**(4), 19-31.

Ni, S.H., Yang, Y.Z. and Lyu, C.R. (2017), "Application of wavelet transform for the impulse response of pile", *Smart Struct. Syst., Int. J.*, **19**(5), 513-521. https://doi.org/10.12989/sss.2017.19.5.513

Ozcan, G., Kocak, Y. and Gulbandilar, E. (2017), "Estimation of compressive strength of BFS and WTRP blended cement mortars with machine learning models", *Comput. Concrete, Int. J.*, **19**(3), 275-282. https://doi.org/10.12989/cac.2017.19.3.275

Park, H., Lee, S.R., Yoon, S. and Choi, J.C. (2013), "Evaluation of thermal response and performance of PHC energy pile: field experiments and numerical simulation", *Appl. Energy*, **103**, 12-24. https://doi.org/10.1016/j.apenergy.2012.10.012

Randolph, M.F. and Murphy, B.S. (1985), "Shaft capacity of driven piles in clay", *Proceedings of the 17th Annual Offshore Technology Conference*, Houston, TX, USA, pp. 371-378.

Sardehaei, E.A., Mehrjardi, G.T. and Dawson, A. (2019), "Full-scale investigations into installation damage of nonwoven geotextiles", *Geomech. Eng., Int. J.*, **17**(1), 81-95. https://doi.org/ 10.12989/gae.2019.17.1.081

Shen, S.L., Wu, H.N., Cui, Y.J. and Yin, Z.Y. (2014), "Long-term settlement behaviour of metro tunnels in the soft deposits of Shanghai", *Tunnell. Undergr. Space Technol.*, **40**, 309-323. https://doi.org/10.1016/j.tust.2013.10.013

Tang, L.B., Ma, Y.B., Wang, L., Zhang, W.G., Zheng, L.N. and Wen, H.J. (2021), "Application of Long Short-Term Memory Neural Network and Prophet algorithm in Slope Displacement Prediction", *Int. J. Geoeng. Case Histories*, **6**(4), 48-66. http://dx.doi.org/10.4417/IJGCH-06-04-04

Teh, C.I., Wong, K.S., Goh, A.T.C. and Jaritngam, S. (1997), "Prediction of pile capacity using neural networks", *J. Comput. Civil Eng., ASCE*, **11**(2), 129-138. https://doi.org/10.1061/(ASCE)0887-3801(1997)11:2(129)

Wang, K. and Sun, W.C. (2018), "A multiscale multi-permeability poroplasticity model linked by recursive homogenizations and deep learning", *Comput. Methods Appl. Mech. Eng.*, **334**, 337-380. https://doi.org/10.1016/j.cma.2018.01.036

Wang, Z.F., Shen, J.S. and Cheng, W.C. (2018), "Simple method to predict ground displacements caused by installing horizontal jet-grouting columns", *Mathe. Problems Eng.*, ID 1897394. https://doi.org/10.1155/2018/1897394

Wang, X.W., Yang, T.L., Xu, Y.S. and Shen, S.L. (2019a), "Evaluation of optimized depth of waterproof curtain to mitigate negative impacts during dewatering", *J. Hydrol.*, **577**(2019), 123969. https://doi.org/10.1016/j.jhydrol.2019.123969

Wang, W.D., Ling, Z., Wu, J.B. and Yuan, J.Y. (2019b), "Field study on bearing characteristics of pre-bored precast pile with enlarged base in Shanghai", *J. Build. Struct.*, **40**(2), 238-245. [In Chinese] https://doi.org/10.14006/j.jzjgxb.2019.02.023

Wu, Y.X., Shen, S.L., Lyu, H.M. and Zhou, A.N. (2020), "Analyses of leak-age effect of waterproof curtain during excavation dewatering", *J. Hydrol.*, **583**, 124582. https://doi.org/10.1016/j.jhydrol.2020.124582

Ye, X., Lyu, Z. and Foong, L.K. (2020), "Hybridized dragonfly, whale and ant lion algorithms in enlarged pile's behavior", *Smart Struct. Syst., Int. J.*, **25**(6), 765-778. https://doi.org/10.12989/sss.2020.25.6.765

Zhang, R.R. (2008), "A simple approach for quality evaluation of non-slender, cast-in-place piles", *Smart Struct. Syst., Int. J.*, **4**(1), 1-17. https://doi.org/10.12989/sss.2008.4.1.001

Zhang, N., Shen, S.L., Wu, H.N., Chai, J.C., Xu, Y.S. and Yin, Z.Y. (2015), "Evaluation of effect of basal geotextile reinforcement under embankment loading on soft marine deposits", *Geotext. Geomembr.*, **43**(6), 506-514. https://doi.org/10.1016/j.geotexmem.2015.05.005

Zhang, N., Shen, S.L., Zhou, A.N. and Xu, Y.S. (2019), "Investigation on performance of neural network using quadratic relative error cost function", *IEEE Access*, **7**, 106642-106652, https://doi.org/10.1109/ACCESS.2019.2930520

Zhang, W., Zhang, R., Wu, C., Goh, A.T.C., Lacasse, S., Liu, Z. and Liu, H. (2020a), "State-of-the-art review of soft computing applications in underground excavations", *Geosci. Frontiers*, **11**(4), 1095-1106. https://doi.org/10.1016/j.gsf.2019.12.003

Zhang, W.G., Li, H.R., Wu, C.Z., Li, Y.Q., Liu, Z.Q. and Liu, H.L. (2020b), "Soft computing approach for prediction of surface settlement induced by earth pressure balance shield tunneling", *Undergr. Space*, **6**(4), 353-363. https://doi.org/10.1016/j.undsp.2019.12.003

Zhang, W.G., Wu, C.Z., Zhong, H.Y., Li, Y.Q. and Wang, L. (2021a), "Prediction of undrained shear strength using extreme gradient boosting and random forest based on Bayesian optimization", *Geosci. Frontiers*, **12**(1), 469-477. https://doi.org/10.1016/j.gsf.2020.03.007

Zhang, W.G., Li, H.R., Li, Y.Q., Liu, H.L., Chen, Y.M. and Ding, X.M. (2021b), "Application of deep learning algorithms in geotechnical engineering: a short critical review", *Artif. Intell. Rev.*, **54**(8), 5633-5673. https://doi.org/10.1007/s10462-021-09967-1

Zhang, W.G., Wu, C.Z., Li, Y.Q., Wang, L. and Samui, P. (2021c), "Assessment of pile drivability using random forest regression and multivariate adaptive regression splines", *Georisk: Assessment and Management of Risk for Engineered Systems*

and Geohazards, **15**(1), 27-40. https://doi.org/10.1080/17499518.2019.1674340

Zhang, N., Shen, S.L., Zhou, A. and Jin, Y.F. (2021d), "Application of LSTM approach for modelling stress–strain behaviour of soil", *Appl. Soft Comput*., **100**, 106959. https://doi.org/10.1016/j.asoc.2020.106959

Zhou, J., Gong, X., Wang, K., Zhang, R. and Yan, T. (2014), "Application of static drill rooted precast nodular pile in soft soil foundation and calculation for bearing capacity", *Chinese J. Rock Mech. Eng.*, **33**(2), 4359-4366. https://doi.org/10.13722/j.cnki.jrme.2014.s2.121

Zhou, M., Liu, H., Hossain, M.S., Hu, Y. and Zhang, T. (2016), "Numerical simulation of plug formation during casing installation of cast-in-place concrete pipe (PCC) piles", *Can. Geotech. J.*, **53**(7), 1-17. https://doi.org/10.1139/cgj-2015-0162

HJ